HHS Public Access

Author manuscript

Oncogene. Author manuscript; available in PMC 2014 February 28.

Published in final edited form as:

Oncogene. 2013 August 29; 32(35): 4078–4085. doi:10.1038/onc.2012.421.

Brain and Testicular Tumors in Mice with Progenitor Cells Lacking BAX and BAK

Samuel G. Katz, M.D., Ph.D.[1,2], **Jill K. Fisher**[1], **Mick Correll, Ph.D.**[3], **Roderick T. Bronson, D.V.M.**[4], **Keith L. Ligon, M.D., Ph.D.**[2,4,5], and **Loren D. Walensky, M.D., Ph.D.**[1]

[1]Department of Pediatric Oncology and the Program in Cancer Chemical Biology, Dana-Farber Cancer Institute, Boston, MA, USA

[2]Department of Pathology, Brigham and Women's Hospital, Boston, MA, USA

[3]Biostatistics and Computational Biology, Dana-Farber Cancer Institute, Boston, MA, USA

[4]Department of Pathology, Harvard Medical School, Boston, MA, USA

[5]Department of Medical Oncology and the Center for Molecular Oncologic Pathology, Dana-Farber Cancer Institute, Harvard Medical School, Boston, MA, USA

Abstract

The pro-apoptotic BCL-2 family proteins BAX and BAK serve as essential gatekeepers of the intrinsic apoptotic pathway and, when activated, transform into pore forming homo-oligomers that permeabilize the mitochondrial outer membrane. Deletion of *Bax* and *Bak* causes marked resistance to death stimuli in a variety of cell types. $Bax^{-/-}Bak^{-/-}$ mice are predominantly nonviable and survivors exhibit multiple developmental abnormalities characterized by cellular excess, including accumulation of neural progenitor cells in the periventricular, hippocampal, cerebellar, and olfactory bulb regions of the brain. To explore the long-term pathophysiologic consequences of BAX/BAK deficiency in a stem cell niche, we generated $Bak^{-/-}$ mice with conditional deletion of *Bax* in Nestin-positive cells. Aged $Nestin^{Cre}Bax^{fl/fl}Bak^{-/-}$ mice manifest progressive brain enlargement with a profound accumulation of NeuN- and Sox2-positive neural progenitor cells within the subventricular zone. One-third of the mice develop frank masses comprised of neural progenitors, and in 20% of these cases, more aggressive, hypercellular tumors emerged. Unexpectedly, 60% of $Nestin^{Cre}Bax^{fl/fl}Bak^{-/-}$ mice harbored high-grade tumors within the testis, a peripheral site of Nestin expression. This *in vivo* model of severe apoptotic blockade highlights the constitutive role of BAX/BAK in long-term regulation of Nestin-positive progenitor cell pools, with loss of function predisposing to adult-onset tumorigenesis.

To whom correspondence should be addressed: Loren D. Walensky, M.D., Ph.D., Dana-Farber Cancer Institute, 450 Brookline Avenue, Mayer 664, Boston, MA 02215, Office: 617-632-6307, Fax: 617-582-8240, Loren_Walensky@dfci.harvard.edu.

Conflict of Interest

The authors have no competing financial interests related to the work described in this manuscript.

Keywords

BAX; BAK; neural progenitor cell; apoptosis; tumorigenesis

Introduction

Programmed cell death plays an essential role during development and homeostasis by eliminating superfluous or damaged cells. The pro- and anti-apoptotic members of the BCL-2 family integrate internal and external stress stimuli to arrive at a life or death decision for the cell (1). BAX and BAK are the two key executioner proteins of the mitochondrial apoptotic pathway (2). When activated by persistent stress signaling, BAX and BAK transform from a monomeric state into homo-oligomers that pierce the mitochondrial outer membrane and release apoptogenic factors, which drive the caspase cascade (3). Whereas cells and tissues deficient in BAX or BAK preserve apoptotic function due to apparent functional redundancy, double deficiency leads to profound apoptotic resistance (4). Indeed, only mice deficient in both *Bax* and *Bak* are embryonic lethal and the minority that do survive exhibit cellular excess in discrete tissues (4). Observed abnormalities in $Bax^{-/-}Bak^{-/-}$ mice include (1) retention of interdigital webs, (2) failure to develop an external vaginal introitus, (3) lymphoid accumulation as reflected by leukocytosis, splenomegaly, lymphadenopathy, and parenchymal infiltrates, and (4) neural progenitor cell hypercellularity within the subventricular zone, hippocampus, cerebellum and olfactory bulb. This constellation of developmental and homeostatic defects highlights the critical roles of BAX/BAK-mediated apoptosis in maintaining the functional integrity of cells and tissues.

Deregulation of the BCL-2 family interaction network has emerged as a contributing etiology for a host of human diseases characterized by either pathologic cellular excess (e.g. cancer) or cellular deficiency (e.g. neurodegeneration). Overexpression of BCL-2 family anti-apoptotic proteins is well known to drive the development, maintenance, and chemoresistance of human cancer (5). Although less common, genetic deletion or mutation of BCL-2 family pro-apoptotic proteins has also been implicated in tumorigenesis. In mice, *Bax* deletion potentiates SV40 T121-induced tumors of the choroid plexus (6), C3(1)/SV40 large T antigen-induced mammary tumors (7), and Myc-induced pancreatic β cell tumors (8). Deletion of *Bax* and *Bak* cooperates with E1A and dominant negative p53 to transform primary baby mouse kidney epithelial cells into highly invasive carcinomas (9), and with mutant $Kras^{G12D}$ to generate sinonasal adenocarcinomas (10). In humans, *Bax* loss-of-function mutations occur in 50% of mismatch mutation repair colon adenocarcinomas (11) and in 20% of cell lines derived from a broad spectrum of human hematopoietic malignancies (12). Interestingly, expression of Baxψ, a more potent inducer of apoptosis than Baxα, occurs within 25% of human glioblastomas and both retards tumor growth in xenograft models and correlates with longer patient survival (13). Thus, as the essential gateway to mitochondrial apoptosis, BAX and BAK appear to directly impact the dynamics of murine and human tumorigenesis.

Given the clinical consequences of severe apoptotic blockade, most notably in oncogenesis, chemoresistance, and cancer relapse, we sought to examine the impact of BAX/BAK deficiency in aged mice, overcoming the embryonic lethality of *Bax*/*Bak* deletion by use of conditional *Bax* deletion in a $Bak^{-/-}$ background. We focused in particular on examining the contribution of apoptosis suppression within the neural stem cell niche to adult-onset tumorigenesis. Whereas BAX and BAK are known to limit the size of the neural stem cell pool (14), the link between a deactivated mitochondrial apoptosis gateway and the development of stem cell-driven cancer remain unknown. Here, we find that conditional deletion of *Bax* in the Nestin-positive cells of $Bak^{-/-}$ mice gives rise to progressive neural progenitor cell hyperplasia and frank brain tumors, in addition to a highly undifferentiated and aggressive neoplasm of the testis, a peripheral site of stem cell-associated Nestin expression.

Results

Progressive megalencephaly in $Nestin^{Cre}Bax^{fl/fl}Bak^{-/-}$ mice

While the majority of $Bax^{-/-}Bak^{-/-}$ mice die *in utero*, rare survivors live long enough to develop accumulations of neural progenitor cells within the subventricular zone (SVZ), hippocampus, cerebellum and olfactory bulb of the brain (4, 14). To investigate the long-term consequences of this aberrant stem cell niche expansion, we bred mice with a germline deletion of *Bak* (4) to animals bearing a floxed (fl) conditional allele of *Bax* (15), which was then deleted by Cre recombinase under control of the rat *Nestin* promoter to yield a central nervous system deficient in BAX and BAK (16). Strikingly, *Bax*/*Bak* deletion produced an overall 34% increase in brain weight compared to wild-type mice (Figure 1A). A statistically significant gene dosage effect was observed with step-wise progression in severity of megalencephaly from $Bak^{-/-}$, $Nestin^{Cre}Bax^{fl/fl}$, $Nestin^{Cre}Bax^{fl/fl}Bak^{+/-}$, to $Nestin^{Cre}Bax^{fl/fl}Bak^{-/-}$. For $Bak^{-/-}$ and $Nestin^{Cre}Bax^{fl/fl}Bak^{-/-}$ brains, which represent the two ends of the spectrum, brain enlargement was grossly evident when comparing age-matched mice (Figure 1B). Notably, the megalencephaly of $Nestin^{Cre}Bax^{fl/fl}Bak^{-/-}$ mice progressed even into old age, as manifested by a statistically significant and stepwise increase in brain weights across <8, 8–15, and 15–20 month old age groups (Figure 1C). These data highlight that deletion of *Bax*/*Bak* in Nestin-positive neural stem cells alters the homeostatic set point for brain size, resulting in progressive brain enlargement throughout the adult life span.

Subventricular zone and rostral migratory stream are predominant sites of neuronal hyperplasia in $Nestin^{Cre}Bax^{fl/fl}Bak^{-/-}$ mice

To determine the histologic drivers of megalencephaly in $Nestin^{Cre}Bax^{fl/fl}Bak^{-/-}$ mice, we examined hematoxylin and eosin (H&E)-stained brain sections across age groups. Like globally-deleted $Bax^{-/-}Bak^{-/-}$ mice (4), $Nestin^{Cre}Bax^{fl/fl}Bak^{-/-}$ animals exhibited neural progenitor cell expansion within the SVZ. However, given the extended life span of $Nestin^{Cre}Bax^{fl/fl}Bak^{-/-}$ animals, the hypercellularity was observed to progress substantially over time, with accumulations along the rostral migratory stream mirroring the natural maturation pathway of types B, C, and A neural progenitors from SVZ to olfactory bulb (Figure 1D–F, Supplementary Figure 1). Interestingly, the degree of SVZ and rostral

migratory stream cellularity corresponded to the severity of megalencephaly observed across genetic subtypes (Figure 1A, D–F, Supplementary Figure 1).

The cells occupying this neurogenic migratory path indeed resemble neural progenitor cells, manifesting round to oval nuclei, condensed chromatin, indistinct nucleoli, and scant cytoplasm. Within the overpopulated regions, cells are Sox2- and NeuN- positive, and Olig2- and EGFR-negative, as assessed by immunohistochemistry (Figure 1G–I, Supplementary Figure 2). Consistent with the genetic defect in apoptosis, Ki-67 (Mib-1) and TUNEL staining are negligible, reflective of low proliferative and apoptotic indices, respectively. Higher power inspection revealed that the aberrant cells formed circular structures resembling Homer Wright pseudo-rosettes (Figure 1J and 1K). This pattern of cellular growth, which ranged from small rosettes formed by relatively few cells to giant rosettes composed of concentric cellular sheets, was observed in 85% of *Nestin*^{Cre}*Bax*$^{fl/fl}$*Bak*$^{-/-}$ mice (28/33). The prevalence of rosetting increased over time, with 60% of 8–12 month old, 75% of 12–16 month old, and 100% of 16–20 month old mouse brain specimens demonstrating the distinctive growth pattern. The presence of rosettes likewise correlated with elevated brain weight (Figure 1L). Immunohistochemical analysis confirmed that the pale centers of pseudo-rosettes contain neuropil, which stained positive for synaptophysin and MAP2, but negative for GFAP (Supplementary Figure 3).

Brain tumorigenesis in Nestin^{Cre}Bax$^{fl/fl}$Bak$^{-/-}$ mice

One-third of *Nestin*^{Cre}*Bax*$^{fl/fl}$*Bak*$^{-/-}$ mice developed large, round, and well-circumscribed masses subjacent to the hippocampus, substantially displacing normal brain tissue (Figure 2A,B, Supplementary Figure 4). Indeed, brain weights of tumor-bearing mice were 27% greater than those of *Nestin*^{Cre}*Bax*$^{fl/fl}$*Bak*$^{-/-}$ mice without brain masses (Supplementary Figure 5). The localization of tumors was consistent with an observed aberrant migration of neural progenitor cells from the SVZ to the sub-hippocampal region in a subset of mice without frank brain tumors (Supplementary Figure 6). No masses were found in any age-matched, littermate control mice including *Bak*$^{-/-}$ mice (n=10), *Nestin*^{Cre}*Bax*$^{fl/fl}$ mice (n=7), or even *Nestin*^{Cre}*Bax*$^{fl/fl}$*Bak*$^{+/-}$ mice (n=10).

The tumors of *Nestin*^{Cre}*Bax*$^{fl/fl}$*Bak*$^{-/-}$ mice contained giant pseudo-rosettes (Figure 2C), whose neuropil-filled centers were positive for MAP2 and synaptophysin (Figure 2D, Supplementary Figure 7). Interestingly, the tumor cells displayed more differentiated features than the progenitor cell expansions of non-tumor bearing mice, as evidenced by increased cellular cytoplasm and the occasional presence of terminally differentiated neurons (Supplementary Figure 8). Whereas the cells remained positive for NeuN and negative for Olig2 and GFAP, with a low Ki-67 proliferation index, Sox2 immunostaining was substantially decreased, consistent with the more differentiated histologic appearance of the tumors compared to the progenitor cell hyperplasia (Figure 2E–H, Supplementary Figure 9A).

Twenty percent of *Nestin*^{Cre}*Bax*$^{fl/fl}$*Bak*$^{-/-}$ brain tumors manifested aggressive, hypercellular, and infiltrative features, with gross head deformity and notable midline shift (Figure 3A–D). The tumors were comprised of dense cellular sheets of small, round- to spindle-shaped, blue cells with scant cytoplasm (Figure 3E–G). Infiltrating cells were

observed at the tumor edges, within the subarachnoid space, and at non-contiguous distal sites. Although small pseudo-rosettes were occasionally observed, the tumor cells predominantly grew in an angiocentric pattern with perivascular cuffing and associated satellitosis. Whereas the tumor cells were positive for NeuN and Sox2, and negative for GFAP, like the neural progenitor cells, a large subset also expressed Olig2 (Figure 3H-*J*, Supplementary Figure 9B), a neural stem cell transcription factor that regulates fate specification of motor neurons and oligodendroglia, and is commonly expressed in human gliomas (17, 18). In contrast to the benign-appearing tumors (Figure 2H), the aggressive masses demonstrated a correspondingly high Ki-67 proliferation index (Figure 3K). Consistent with the neuronal deletion of *Bax* and *Bak*, the presence of apoptotic bodies was strikingly absent from the tumor tissue.

Testicular tumorigenesis in Nestin^{Cre}Bax$^{fl/fl}$Bak$^{-/-}$ mice

In surveying peripheral tissues that express Nestin (19), we surprisingly identified high-grade testicular masses in 63% (12 of 19) of the *Nestin*^{Cre}*Bax*$^{fl/fl}$*Bak*$^{-/-}$ mice, 20% (1 of 5) of age-matched *Nestin*^{Cre}*Bax*$^{fl/fl}$*Bak*$^{+/-}$ mice, and in no (0 of 17) *Bak*$^{-/-}$ mice (Supplementary Figure 10). The tumors exhibited highly undifferentiated and aggressive features, with pleomorphic cell morphology, numerous mitoses, and occasional giant cell formation (Figure 4*A*–*C*). Whereas global *Bax*$^{-/-}$ mice are infertile due to failed sperm maturation as a consequence of Sertoli cell exhaustion from surplus premeitoic germ cells (20), *Nestin*^{Cre}*Bax*$^{fl/fl}$*Bak*$^{-/-}$ mice displayed normal spermatogenesis (Figure 4*D*). Although the highly undifferentiated appearance of the interstitial tumor cells was suggestive of an immune cell malignancy, the cells were negative for both CD3 and B220 (Supplementary Figure 11).

To investigate the cell of origin for the testicular tumors, we generated *Nestin*^{Cre}*ROSA*^{LacZ} mice and conducted a fate-mapping study that revealed selective LacZ staining of inter-tubular Leydig cells as well as occasional germ cells, but no labeling of control *ROSA*^{LacZ} testis (Figure 4E,F). Nestin expression within the testis has previously been localized to vascular progenitor cells, which transdifferentiate to produce Leydig cells (21, 22), and within the germ cell lineage(23).

Gene expression analysis of Nestin^{Cre}Bax$^{fl/fl}$Bak$^{-/-}$ tumors

To distinguish between a germ and Leydig cell of origin for the observed testicular tumors, we performed gene expression analysis on wild-type testes and tumor-bearing *Nestin*^{Cre}*Bax*$^{fl/fl}$*Bak*$^{-/-}$ testes, as confirmed histologically. The expression profile of the tumor-bearing testes matched that of a germ cell signature, rather than that of a Leydig, interstitial, or tubular cell signature, as assessed by gene set enrichment analyses (GSEA) (Figure 5A) (24, 25). Of note, despite containing admixed normal cells, the pathologic *Nestin*^{Cre}*Bax*$^{fl/fl}$*Bak*$^{-/-}$specimens demonstrated decreased *Bax* and *Bak* expression compared to the corresponding wild-type tissue, consistent with deletion of *Bax*/*Bak* in the tumors.

Unbiased GSEA was used to further characterize the testicular tumors. Of 404 stem cell signatures found within the GeneSigDB database, 278 are significantly (FDR $q < 0.25$)

enriched in tumor-bearing *Nestin*^{Cre}*Bax*$^{fl/fl}$*Bak*$^{-/-}$ testes, whereas only 1 signature was significantly enriched in wild-type testes (Figure 5B). The embryonic stem cell signature can be subdivided into distinct subsignatures that include Myc-related factors (Myc module), core pluripotency factors (Core module), and Polycomb complex factors (PrC module), with the Myc module accounting for the predominant similarity of embryonic stem cells to cancer cells (26). Interestingly, the tumor-bearing testes are enriched for both the Myc and Core modules, while the PrC module is repressed (Figure 5C). Whereas cancers typically manifest a Myc up, Core down, and Prc down profile, the added finding of a Core up signature is consistent with the progenitor cell origin of the *Nestin*^{Cre}*Bax*$^{fl/fl}$*Bak*$^{-/-}$ testes tumors. Likewise, using the classification of Ben-Porath et al. (27), tumor-bearing *Nestin*^{Cre}*Bax*$^{fl/fl}$*Bak*$^{-/-}$ testes were enriched for Myc target gene sets, and Nanog, Oct4 and Sox2 targets (Core factors), but not for H3K27 bound, suz12, and PRC2 targets (Polycomb factors) (Supplementary Figure 12).

Finally, we created a gene signature by barcode analysis of a highly aggressive brain tumor that emerged from a *Nestin*^{Cre}*Bax*$^{fl/fl}$*Bak*$^{-/-}$ mouse and for *Nestin*^{Cre}*Bax*$^{fl/fl}$*Bak*$^{-/-}$ brains bearing extensive SVZ proliferations. In both cases, the gene signatures were highly enriched in tumor-bearing *Nestin*^{Cre}*Bax*$^{fl/fl}$*Bak*$^{-/-}$ testes (Figure 5D). Thus, we find that deletion of *Bax* and *Bak* in the Nestin-positive progenitor cells of the testis likewise gives rise to tumors with stem cell characteristics in adult mice.

Discussion

The adult brain retains a pool of repopulating neural progenitors cells that reside in the perivascular niche of the SVZ and migrate along the rostral migratory stream to the olfactory bulb and to sites of injury (28). The long-term self-renewal capacity of such cell populations within the brain represents a potential vulnerability for oncogenesis should the critical balance between progenitor cell life, death, and differentiation become deregulated. Although loss of p53 alone within the SVZ is not sufficient for tumor formation, the proliferative advantage leads to hypercellularity, rapid differentiation, and increased p53-independent apoptosis (29), highlighting that p53 restrains the adult neural stem cell pool (30). The combined loss of p53 with other neural stem cell regulators, such as PTEN, trigger frank neoplastic transformation (31). Like loss of p53, combined *Bax*/*Bak* deletion revealed a key role for these multidomain pro-apoptotic members of the BCL-2 family in regulating the size of the neural stem cell pool (4). However, unlike the capacity of *p53*$^{-/-}$ cells to engage a p53-independent apoptotic pathway, *Bax*$^{-/-}$*Bak*$^{-/-}$ cells sustain a profound block in apoptosis (2). Whereas such a severe apoptotic defect in self-renewing neural progenitor cells would be expected to predispose to brain tumorigenesis, the embryonic lethality of *Bax*$^{-/-}$*Bak*$^{-/-}$ mice and foreshortened lifespan of the limited survivors precluded longitudinal analysis. To circumvent this limitation and examine the oncogenic impact of deleting *Bax*/*Bak* in a stem cell niche, we generated and characterized *Nestin*^{Cre}*Bax*$^{fl/fl}$*Bak*$^{-/-}$ mice as a model for progenitor cell-driven tumorigenesis.

We find that preventing Nestin-positive neural progenitor cell apoptosis through targeted *Bax*/*Bak* deletion gives rise to substantial and progressive hypercellularity both within and emerging from the SVZ. In a subset of mice, the progenitor cell hyperplasia and aberrant

migratory activity give rise to frank sub-hippocampal tumors. Interestingly, the observed rosetting pattern of neurocytic growth is found in several human cancers, yet the emergence of this pattern in mice is strikingly rare (32). For example, the constellation of neurocytic cells, abundant neoplastic neuropil, and rosette pattern of growth is most similar to embryonic neurogenic tumors of childhood, such as cerebral neuroblastoma and embryonal tumor with abundant neuropil and true rosettes (ETANTR) (33, 34). Rosette forming glioneuronal tumors of the ventricular system (RGNT) shares the features of tumor location and presence of rosettes(35). Whereas the hyperplastic progenitor cells in non-tumor bearing mice manifest NeuN and Sox2 immunoreactivity, the large tumors that take hold outside of the stem cell niche contain more differentiated neurons that lose Sox2 positivity, consistent with initiation of a mature neuronal differentiation program upon emigration from the stem cell niche (36). The development of highly aggressive brain tumors in a smaller subset of $Nestin^{Cre}Bax^{fl/fl}Bak^{-/-}$ mice underscores the malignant potential of neural progenitors that lack an intact mitochondrial apoptotic pathway. These highly infiltrative tumors retain NeuN and Sox2 positivity, and also express Olig2, a transcription factor that is highly expressed in brain cancer stem cells, required for neural progenitor cell proliferation, and a potent suppressor of p53 activity (17, 18).

In addition to brain tumorigenesis, $Nestin^{Cre}Bax^{fl/fl}Bak^{-/-}$ mice manifest a highly penetrant cancer of the testis. Like the SVZ, the testis contains a Nestin-positive stem cell niche. Excision of $Bax^{fl/fl}$ in the germ cell compartment by $Nestin^{Cre}$ is supported both by prior reports of $Nestin^{Cre}$ activity in germ cells(23) and our *LacZ* fate mapping experiments. In contrast to mice with global *Bax* deletion, intratubular spermatogenesis appears normal in $Nestin^{Cre}Bax^{fl/fl}Bak^{-/-}$ testis, consistent with the observed sporadic expression of $Nestin^{Cre}$ within the germ cell compartment. The testicular architecture of tumor-bearing $Nestin^{Cre}Bax^{fl/fl}Bak^{-/-}$ testis is completely effaced by highly pleomorphic and proliferative cells. Although the bulk of tumor cells reside in and infiltrate the interstitium, the cellular cytology and gene expression analyses support a germ cell origin. The gene expression analyses further revealed that tumor-bearing $Nestin^{Cre}Bax^{fl/fl}Bak^{-/-}$ testes manifest robust cancer and stem cell signatures, in addition to sharing gene expression features with $Nestin^{Cre}Bax^{fl/fl}Bak^{-/-}$ neural progenitor hyperplasia and tumors. The commonalities shared by $Bax^{-/-}Bak^{-/-}$ progenitors and cancer stem cells, including the capacity for self-renewal and profound apoptotic resistance, underscore the utility of this mouse model in delineating the additional genetic factors that drive discrete subtypes of cancer and what therapeutic modalities will be required to overcome them.

Materials and Methods

Mice

$Nestin^{Cre}Bax^{fl/fl}Bak^{-/-}$ mice were generated from $Bak^{-/-}$, $Bax^{fl/fl}$ and $Nestin^{Cre}$ animals as described (16). $Nestin^{Cre}ROSA^{LacZ}$ mice for fate-mapping analysis was generated from $Nestin^{Cre}$ and FVB.129S4(B6)-Gt(ROSA)26Sor^{tm1Sor}/J animals (Jackson Laboratories). All animal experiments were performed in accordance with NIH guidelines and approved by the Dana-Farber Cancer Institute Institutional Animal Care and Use Committee.

Histology and Immunohistochemistry

Mouse tissues were fixed in either Bouin's or 10% formalin for greater than 24 hours, passed through graded alcohols, and embedded in paraffin. Slides containing 5 μm thick sections were used for hematoxylin and eosin staining, or immunohistochemistry. Slides were soaked in xylene, passed through graded alcohols, and immersed in distilled water. Immunohistochemistry was performed using the following conditions: (1) pressure cooker antigen retrieval (0.01 M citrate buffer, pH 6.0) followed by antibodies to GFAP (1:20,000; Z0334, DAKO), Olig2 (1:500; AB9610, Millipore), Sox2 (1:100; 3579, Cell Signaling), NeuN (1:7,500; MAB377, Chemicon), and MAP2 (1:5000; M4403, Sigma), (2) pressure cooker antigen retrieval (EDTA buffer, pH 8.0) followed by Ki-67 immunostaining (1:250; VP-RM04, Vector), (3) anti-synaptophysin immunostaining (1:100; 180130, Invitrogen) without antigen retrieval, or (4) ten minute proteinase K-based antigen retrieval followed by anti-EGFR immunostaining (1:400; M3563, DAKO). For antibodies generated in mice, a mouse-on-mouse IgG blocking kit (BMK-2202, Vector labs) was employed according to the manufacturer's instructions. TUNEL staining was performed according to the manufacture's protocol (S7100; Millipore Apoptag).

LacZ staining

Mouse tissues were removed and fixed in 4% paraformaledhyde/PBS, rinsed with Buffer A (100 mM sodium phosphate, 2 mM $MgCl_2$, 0.01% sodium deoxycholate and 0.02% NP-40), and stained with 5 mM potassium ferricyanide, 5 mM potassium ferrocyonide and 1 mg/ml X-gal in Buffer A. Tissues were then post-fixed in 10% formalin, embedded in paraffin, and counterstained with neutral fast red (NFR).

Microarray analysis

Brains were cut mid-sagitally and distinct regions removed under a dissection microscope. Testes were flash frozen and cut in half for histology and RNA extraction. Total RNA was extracted from tissues frozen in Trizol (Invitrogen) using Qiagen RNeasy. RNA was reverse transcribed and hybridized to a mouse Gene 1.0 ST chip for the testes samples and to a mouse 430 2.0 full chip for the brain samples at the Dana-Farber Cancer Institute Microarray Core Facility. Array quality was assessed using R/Bioconductor (37). All arrays passed visual inspection and no technical outliers were identified. Transcript level summarization and RMA normalization of CEL files was achieved using the Oligo package (38). To identify genes correlating with the phenotypic groups, we used limma (39) to fit a statistical linear model to the data and then tested for differential gene expression in the contrasts of interest. Results were adjusted for multiple testing using the Benjamini and Hochberg (BH) method (40). Gene set enrichment analysis (GSEA) was performed with the pre-ranked implementation of the GSEA software package(41) using the moderated t-statistic from limma to determine rank order. Tissue specific gene sets for the four different components of the testis were derived from the E-AFFX-5 dataset available at ArrayExpress. Briefly, each of the four testis components was first analyzed individually using Barcode(24) to determine the subset of genes that are expressed in that tissue, and genes that were found to be expressed in all four tissues were excluded. Barcode analysis was similarly used in deriving gene signatures for the aggressive brain tumor and brains

bearing SVZ proliferations, with additional filtering criteria requiring an absolute fold-change greater than two relative to wild-type tissue. Stem cell signatures were identified from the GeneSigDB database(42) and were tested for significance using the CP (v2.5) gene set from MSigDB as background.

Supplementary Material

Refer to Web version on PubMed Central for supplementary material.

Acknowledgements

We thank E. Smith for editorial and graphics assistance, R. Segal, R. Folkerth, and C. Stiles for helpful discussions, and S. Rodig and the Harvard Rodent Histology and Specialized Histopathology cores for technical support. This work was supported by NIH grants 5R01CA050239 and 1P01CA142536 to L.D.W., NIH grant 5K08HL103847 to S.G.K., and the Todd J. Schwartz Memorial Fund.

This work was supported by 5R01CA050239 and 1P01CA142536 (L.D.W.) and 5K08HL103847 (S.G.K.)

References

1. Youle RJ, Strasser A. The BCL-2 protein family: opposing activities that mediate cell death. Nat Rev Mol Cell Biol. 2008; 9(1):47–59. Epub 2007/12/22. [PubMed: 18097445]
2. Wei MC, Zong WX, Cheng EH, Lindsten T, Panoutsakopoulou V, Ross AJ, et al. Proapoptotic BAX and BAK: a requisite gateway to mitochondrial dysfunction and death. Science. 2001; 292(5517):727–730. Epub 2001/04/28. [PubMed: 11326099]
3. Tait SW, Green DR. Mitochondria and cell death: outer membrane permeabilization and beyond. Nat Rev Mol Cell Biol. 2010; 11(9):621–632. Epub 2010/08/05. [PubMed: 20683470]
4. Lindsten T, Ross AJ, King A, Zong WX, Rathmell JC, Shiels HA, et al. The combined functions of proapoptotic Bcl-2 family members bak and bax are essential for normal development of multiple tissues. Mol Cell. 2000; 6(6):1389–1399. Epub 2001/02/13. [PubMed: 11163212]
5. Yip KW, Reed JC. Bcl-2 family proteins and cancer. Oncogene. 2008; 27(50):6398–6406. Epub 2008/10/29. [PubMed: 18955968]
6. Yin C, Knudson CM, Korsmeyer SJ, Van Dyke T. Bax suppresses tumorigenesis and stimulates apoptosis in vivo. Nature. 1997; 385(6617):637–640. Epub 1997/02/13. [PubMed: 9024662]
7. Shibata MA, Liu ML, Knudson MC, Shibata E, Yoshidome K, Bandey T, et al. Haploid loss of bax leads to accelerated mammary tumor development in C3(1)/SV40-TAg transgenic mice: reduction in protective apoptotic response at the preneoplastic stage. EMBO J. 1999; 18(10):2692–2701. Epub 1999/05/18. [PubMed: 10329616]
8. Dansen TB, Whitfield J, Rostker F, Brown-Swigart L, Evan GI. Specific requirement for Bax, not Bak, in Myc-induced apoptosis and tumor suppression in vivo. J Biol Chem. 2006; 281(16):10890–10895. Epub 2006/02/09. [PubMed: 16464852]
9. Degenhardt K, Chen G, Lindsten T, White E. BAX and BAK mediate p53-independent suppression of tumorigenesis. Cancer Cell. 2002; 2(3):193–203. Epub 2002/09/21. [PubMed: 12242152]
10. Kirsch DG, Dinulescu DM, Miller JB, Grimm J, Santiago PM, Young NP, et al. A spatially and temporally restricted mouse model of soft tissue sarcoma. Nat Med. 2007; 13(8):992–997. Epub 2007/08/07. [PubMed: 17676052]
11. Rampino N, Yamamoto H, Ionov Y, Li Y, Sawai H, Reed JC, et al. Somatic frameshift mutations in the BAX gene in colon cancers of the microsatellite mutator phenotype. Science. 1997; 275(5302):967–969. Epub 1997/02/14. [PubMed: 9020077]
12. Meijerink JP, Mensink EJ, Wang K, Sedlak TW, Sloetjes AW, de Witte T, et al. Hematopoietic malignancies demonstrate loss-of-function mutations of BAX. Blood. 1998; 91(8):2991–2997. Epub 1998/05/16. [PubMed: 9531611]
13. Cartron PF, Oliver L, Martin S, Moreau C, LeCabellec MT, Jezequel P, et al. The expression of a new variant of the pro-apoptotic molecule Bax, Baxpsi, is correlated with an increased survival of

glioblastoma multiforme patients. Hum Mol Genet. 2002; 11(6):675–687. Epub 2002/03/26. [PubMed: 11912183]

14. Lindsten T, Golden JA, Zong WX, Minarcik J, Harris MH, Thompson CB. The proapoptotic activities of Bax and Bak limit the size of the neural stem cell pool. J Neurosci. 2003; 23(35): 11112–11119. Epub 2003/12/06. [PubMed: 14657169]
15. Takeuchi O, Fisher J, Suh H, Harada H, Malynn BA, Korsmeyer SJ. Essential role of BAX, BAK in B cell homeostasis and prevention of autoimmune disease. Proc Natl Acad Sci U S A. 2005; 102(32):11272–11277. Epub 2005/08/02. [PubMed: 16055554]
16. Reyes NA, Fisher JK, Austgen K, VandenBerg S, Huang EJ, Oakes SA. Blocking the mitochondrial apoptotic pathway preserves motor neuron viability and function in a mouse model of amyotrophic lateral sclerosis. J Clin Invest. 2010; 120(10):3673–3679. Epub 2010/10/05. [PubMed: 20890041]
17. Ligon KL, Huillard E, Mehta S, Kesari S, Liu H, Alberta JA, et al. Olig2-regulated lineage-restricted pathway controls replication competence in neural stem cells and malignant glioma. Neuron. 2007; 53(4):503–517. Epub 2007/02/14. [PubMed: 17296553]
18. Mehta S, Huillard E, Kesari S, Maire CL, Golebiowski D, Harrington EP, et al. The central nervous system-restricted transcription factor Olig2 opposes p53 responses to genotoxic damage in neural progenitors and malignant glioma. Cancer Cell. 2011; 19(3):359–371. Epub 2011/03/15. [PubMed: 21397859]
19. Amoh Y, Yang M, Li L, Reynoso J, Bouvet M, Moossa AR, et al. Nestin-linked green fluorescent protein transgenic nude mouse for imaging human tumor angiogenesis. Cancer Res. 2005; 65(12): 5352–5357. Epub 2005/06/17. [PubMed: 15958583]
20. Knudson CM, Tung KS, Tourtellotte WG, Brown GA, Korsmeyer SJ. Bax-deficient mice with lymphoid hyperplasia and male germ cell death. Science. 1995; 270(5233):96–99. Epub 1995/10/06. [PubMed: 7569956]
21. Davidoff MS, Middendorff R, Enikolopov G, Riethmacher D, Holstein AF, Muller D. Progenitor cells of the testosterone-producing Leydig cells revealed. J Cell Biol. 2004; 167(5):935–944. Epub 2004/12/01. [PubMed: 15569711]
22. Lobo MV, Arenas MI, Alonso FJ, Gomez G, Bazan E, Paino CL, et al. Nestin, a neuroectodermal stem cell marker molecule, is expressed in Leydig cells of the human testis and in some specific cell types from human testicular tumours. Cell Tissue Res. 2004; 316(3):369–376. Epub 2004/05/06. [PubMed: 15127288]
23. Dubois NC, Hofmann D, Kaloulis K, Bishop JM, Trumpp A. Nestin-Cre transgenic mouse line Nes-Cre1 mediates highly efficient Cre/loxP mediated recombination in the nervous system, kidney, and somite-derived tissues. Genesis. 2006; 44(8):355–360. Epub 2006/07/19. [PubMed: 16847871]
24. McCall MN, Uppal K, Jaffee HA, Zilliox MJ, Irizarry RA. The Gene Expression Barcode: leveraging public data repositories to begin cataloging the human and murine transcriptomes. Nucleic Acids Res. 2011; 39(Database issue):D1011–D1015. Epub 2011/01/05. [PubMed: 21177656]
25. Su AI, Wiltshire T, Batalov S, Lapp H, Ching KA, Block D, et al. A gene atlas of the mouse and human protein-encoding transcriptomes. Proc Natl Acad Sci U S A. 2004; 101(16):6062–6067. Epub 2004/04/13. [PubMed: 15075390]
26. Kim J, Woo AJ, Chu J, Snow JW, Fujiwara Y, Kim CG, et al. A Myc network accounts for similarities between embryonic stem and cancer cell transcription programs. Cell. 2010; 143(2): 313–324. Epub 2010/10/16. [PubMed: 20946988]
27. Ben-Porath I, Thomson MW, Carey VJ, Ge R, Bell GW, Regev A, et al. An embryonic stem cell-like gene expression signature in poorly differentiated aggressive human tumors. Nat Genet. 2008; 40(5):499–507. Epub 2008/04/30. [PubMed: 18443585]
28. Sauvageot CM, Kesari S, Stiles CD. Molecular pathogenesis of adult brain tumors and the role of stem cells. Neurol Clin. 2007; 25(4):891–924. vii. Epub 2007/10/30. [PubMed: 17964020]
29. Gil-Perotin S, Marin-Husstege M, Li J, Soriano-Navarro M, Zindy F, Roussel MF, et al. Loss of p53 induces changes in the behavior of subventricular zone cells: implication for the genesis of glial tumors. J Neurosci. 2006; 26(4):1107–1116. Epub 2006/01/27. [PubMed: 16436596]

30. Meletis K, Wirta V, Hede SM, Nister M, Lundeberg J, Frisen J. p53 suppresses the self-renewal of adult neural stem cells. Development. 2006; 133(2):363–369. Epub 2005/12/22. [PubMed: 16368933]
31. Zheng H, Ying H, Yan H, Kimmelman AC, Hiller DJ, Chen AJ, et al. p53 and Pten control neural and glioma stem/progenitor cell renewal and differentiation. Nature. 2008; 455(7216):1129–1133. Epub 2008/10/25. [PubMed: 18948956]
32. al-Ubaidi MR, Font RL, Quiambao AB, Keener MJ, Liou GI, Overbeek PA, et al. Bilateral retinal and brain tumors in transgenic mice expressing simian virus 40 large T antigen under control of the human interphotoreceptor retinoid-binding protein promoter. J Cell Biol. 1992; 119(6):1681–1687. Epub 1992/12/01. [PubMed: 1334963]
33. Eberhart CG, Brat DJ, Cohen KJ, Burger PC. Pediatric neuroblastic brain tumors containing abundant neuropil and true rosettes. Pediatr Dev Pathol. 2000; 3(4):346–352. Epub 2000/07/13. [PubMed: 10890250]
34. Gessi M, Giangaspero F, Lauriola L, Gardiman M, Scheithauer BW, Halliday W, et al. Embryonal tumors with abundant neuropil and true rosettes: a distinctive CNS primitive neuroectodermal tumor. Am J Surg Pathol. 2009; 33(2):211–217. Epub 2008/11/07. [PubMed: 18987548]
35. Preusser M, Dietrich W, Czech T, Prayer D, Budka H, Hainfellner JA. Rosette-forming glioneuronal tumor of the fourth ventricle. Acta Neuropathol. 2003; 106(5):506–508. Epub 2003/08/14. [PubMed: 12915951]
36. Burness ML, Sipkins DA. The stem cell niche in health and malignancy. Semin Cancer Biol. 2010; 20(2):107–115. Epub 2010/06/01. [PubMed: 20510363]
37. Gentleman RC, Carey VJ, Bates DM, Bolstad B, Dettling M, Dudoit S, et al. Bioconductor: open software development for computational biology and bioinformatics. Genome Biol. 2004; 5(10):R80. Epub 2004/10/06. [PubMed: 15461798]
38. Carvalho BS, Irizarry RA. A framework for oligonucleotide microarray preprocessing. Bioinformatics. 26(19):2363–2367. Epub 2010/08/07. [PubMed: 20688976]
39. Smyth GK. Linear models and empirical bayes methods for assessing differential expression in microarray experiments. Stat Appl Genet Mol Biol. 2004; 3 Article3. Epub 2006/05/02.
40. Benjamini Y, Hochberg Y. Controlling the False Discovery Rate: a Practival and Powerful Approach to Multiple Testing. J R Stat Soc. 1995; 57(1):289–300.
41. Subramanian A, Tamayo P, Mootha VK, Mukherjee S, Ebert BL, Gillette MA, et al. Gene set enrichment analysis: a knowledge-based approach for interpreting genome-wide expression profiles. Proc Natl Acad Sci U S A. 2005; 102(43):15545–15550. Epub 2005/10/04. [PubMed: 16199517]
42. Culhane AC, Schroder MS, Sultana R, Picard SC, Martinelli EN, Kelly C, et al. GeneSigDB: a manually curated database and resource for analysis of gene expression signatures. Nucleic Acids Res. 2012; 40(Database issue):D1060–D1066. Epub 2011/11/24. [PubMed: 22110038]

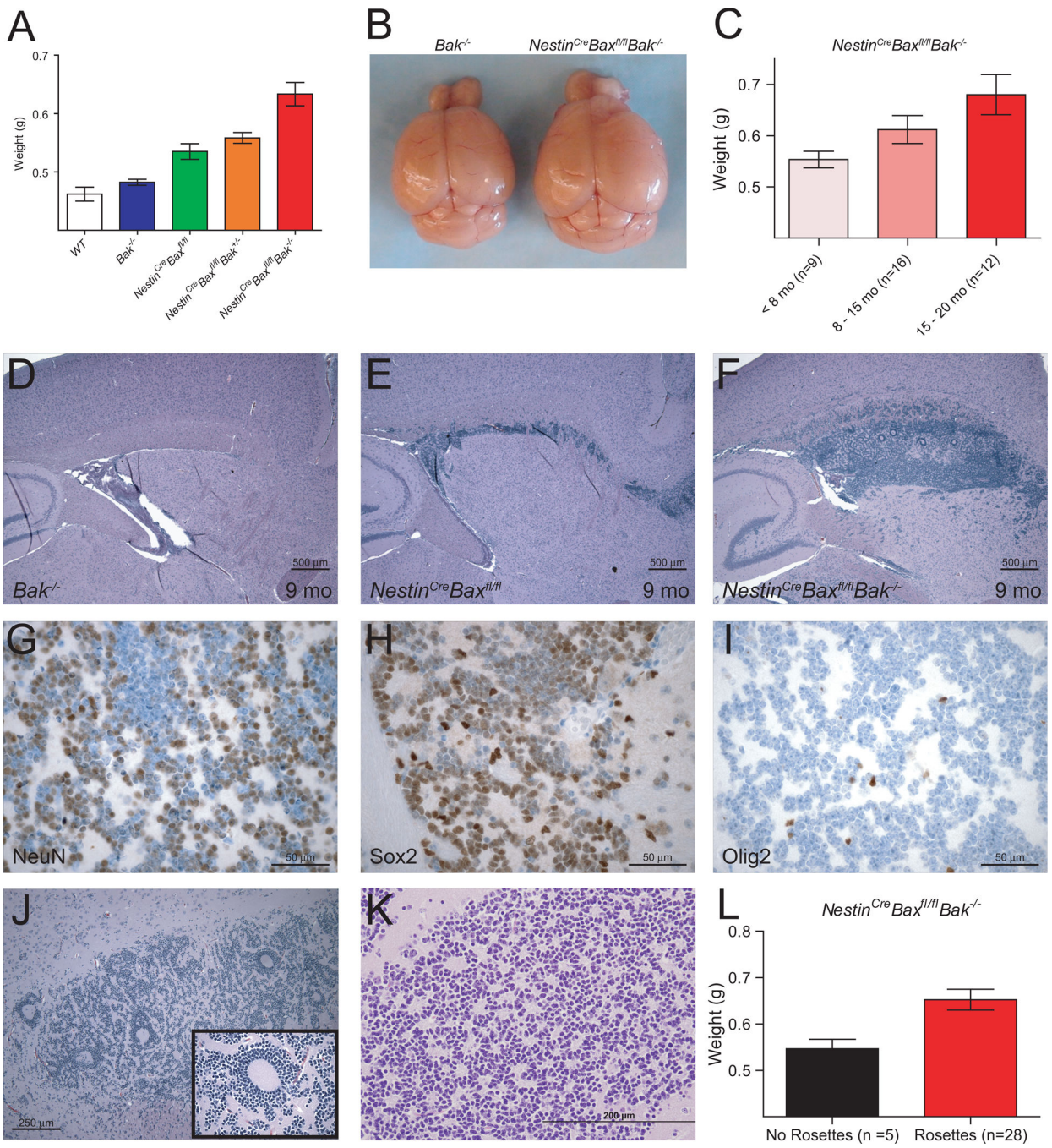

Figure 1.

Progressive megalencephaly with SVZ hyperplasia and Homer-Wright pseudo-rosetting in *Nestin*^{Cre}*Bax*$^{fl/fl}$*Bak*$^{-/-}$ mice. (A) Adult *Nestin*^{Cre}*Bax*$^{fl/fl}$*Bak*$^{-/-}$ mice manifest the heaviest brains among littermate controls, with an observed gene dosage effect (*Nestin*^{Cre}*Bax*$^{fl/fl}$*Bak*$^{-/-}$ [n=46] vs.: WT [n=5], p=0.002; *Bak*$^{-/-}$[n=44], p<0.0001; *Nestin*^{Cre}*Bax*$^{fl/fl}$ [n=8], p=0.037; *Nestin*^{Cre}*Bax*$^{fl/fl}$*Bak*$^{+/-}$ [n=17], p=0.03). Data are mean ± s.d. (B) Representative brains of two age-matched *Bak*$^{-/-}$ and *Nestin*^{Cre}*Bax*$^{fl/fl}$*Bak*$^{-/-}$ mice. (C) Megalencephaly of *Nestin*^{Cre}*Bax*$^{fl/fl}$*Bak*$^{-/-}$ mice progresses with age (15–20 month old

cohort vs. <8 month old cohort, p=0.016). Data are mean ± s.d. (D–F*)* H&E-stained sagittal brain sections demonstrate progressive expansion of the SVZ progenitor cell population, the size of which correlates with the number of *Bax* and *Bak* alleles deleted. (G–I*)* Immunohistochemical analysis of the $Nestin^{Cre}Bax^{fl/fl}Bak^{-/-}$ SVZ region revealed abundant expression of NeuN and Sox2, but little to no staining for Olig2. (J–L) H&E-stained sections demonstrate both giant (J*)* and small (K) rosettes within the SVZ of $Nestin^{Cre}Bax^{fl/fl}Bak^{-/-}$ mice. (L) The presence of rosetting correlates with elevated brain weight (p=0.04). Data are mean ± s.d.

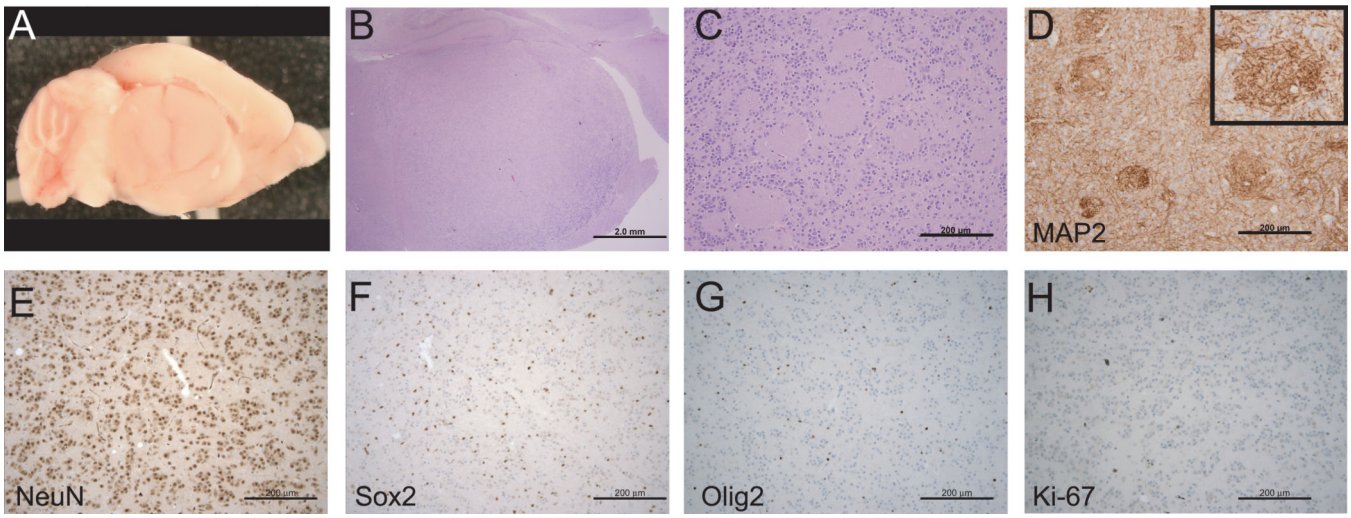

Figure 2.

Brain tumors of *Nestin*^{Cre}*Bax*$^{fl/fl}$*Bak*$^{-/-}$ mice. (A and B) The majority of tumors were large, round, and well-circumscribed masses that extended from the SVZ to the sub-hippocampal region. (C) Tumor tissue contained rosetting neurocytes, neoplastic neuropil, and occasional neurons with differentiated features, including increased cytoplasm. (D) Tumor rosettes contain MAP2-positive neuropil. (*E-H*) Tumor cells are positive for NeuN (E) but negative for Sox2 (F) and Olig2 (G), and exhibit a low Ki-67 proliferation index (*H*).

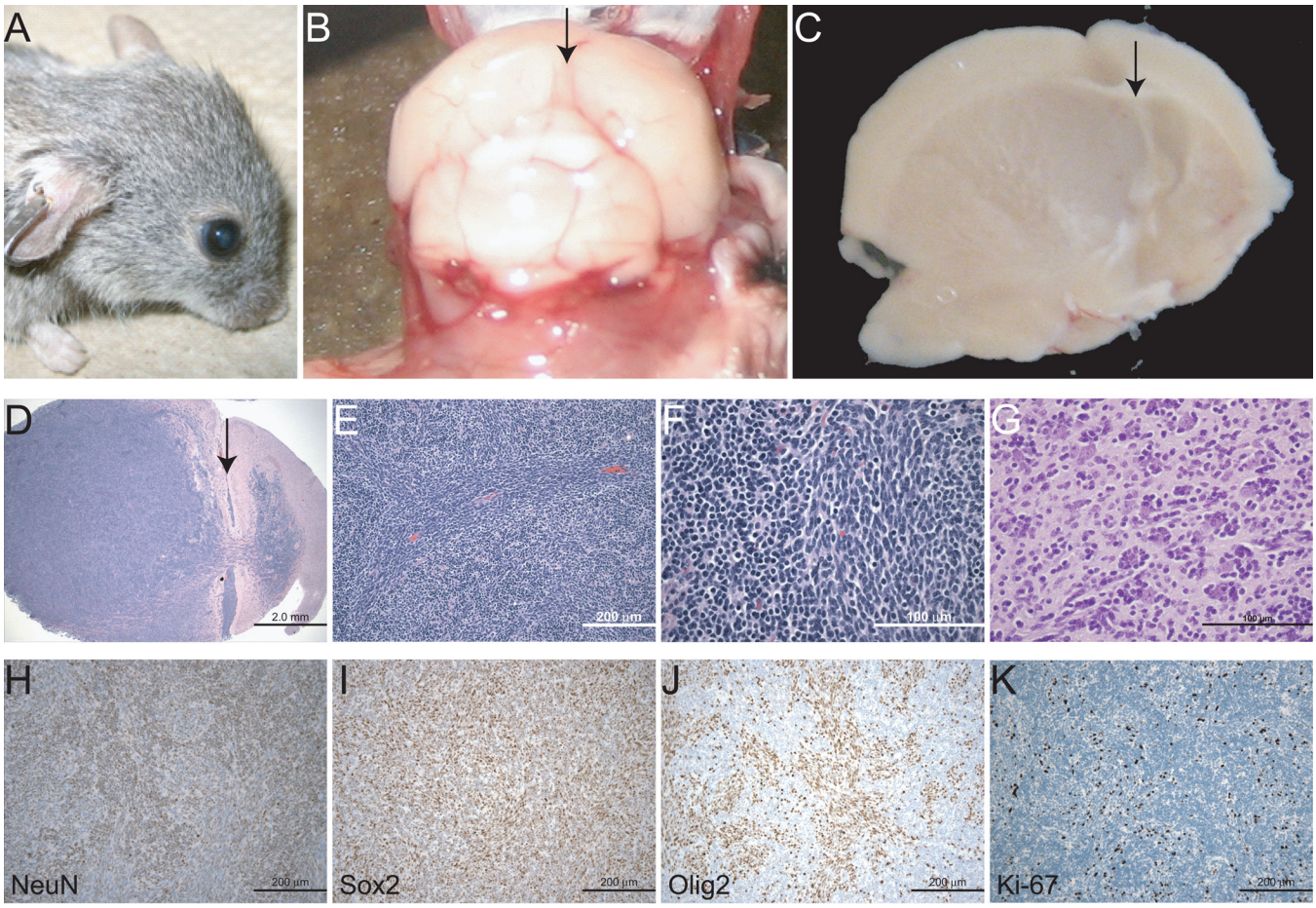

Figure 3.

A subset of *Nestin*^{Cre}*Bax*$^{fl/fl}$*Bak*$^{-/-}$ brain tumors exhibit high grade features. An exemplary aggressive brain tumor was associated with gross head deformity (A) and pronounced compression with midline shift (B and C). Arrow, central sulcus (D–G) H&E-stained sections revealed malignant-appearing cells streaming from the SVZ, with a fasicular growth pattern, perivascular cuffing, mitotic cells, and satellitosis. (H–K) Tumor cells were NeuN- (H), Sox2- (I), and Olig2-positive (J), and exhibited a high Ki-67 proliferation index (K).

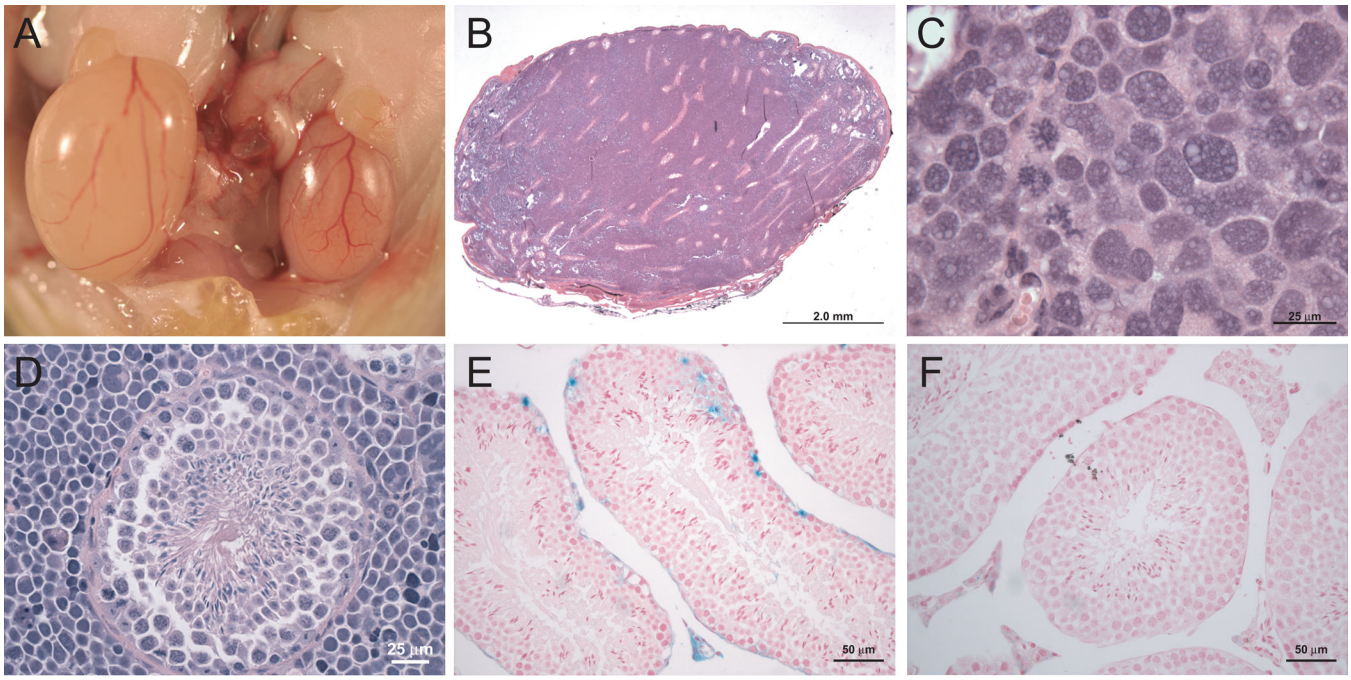

Figure 4.

Testicular tumors of *Nestin*^{Cre}*Bax*$^{fl/fl}$*Bak*$^{-/-}$ mice. (A) Testicular enlargement was evident on necropsy of affected *Nestin*^{Cre}*Bax*$^{fl/fl}$*Bak*$^{-/-}$ mice. (B and C) H&E stained sections demonstrated effacement of testicular architecture by a striking inter-tubular neoplasia. (D) In contrast to *Bax*$^{-/-}$ mice, *Nestin*^{Cre}*Bax*$^{fl/fl}$*Bak*$^{-/-}$ animals displayed normal spermatogenesis. Magnification, *600X* (E and F) The intertubular Leydig cells marked positive in *Nestin*^{Cre}*ROSA*^{LacZ} reporter mice (E), but not in *ROSA*^{LacZ} control animals (F).

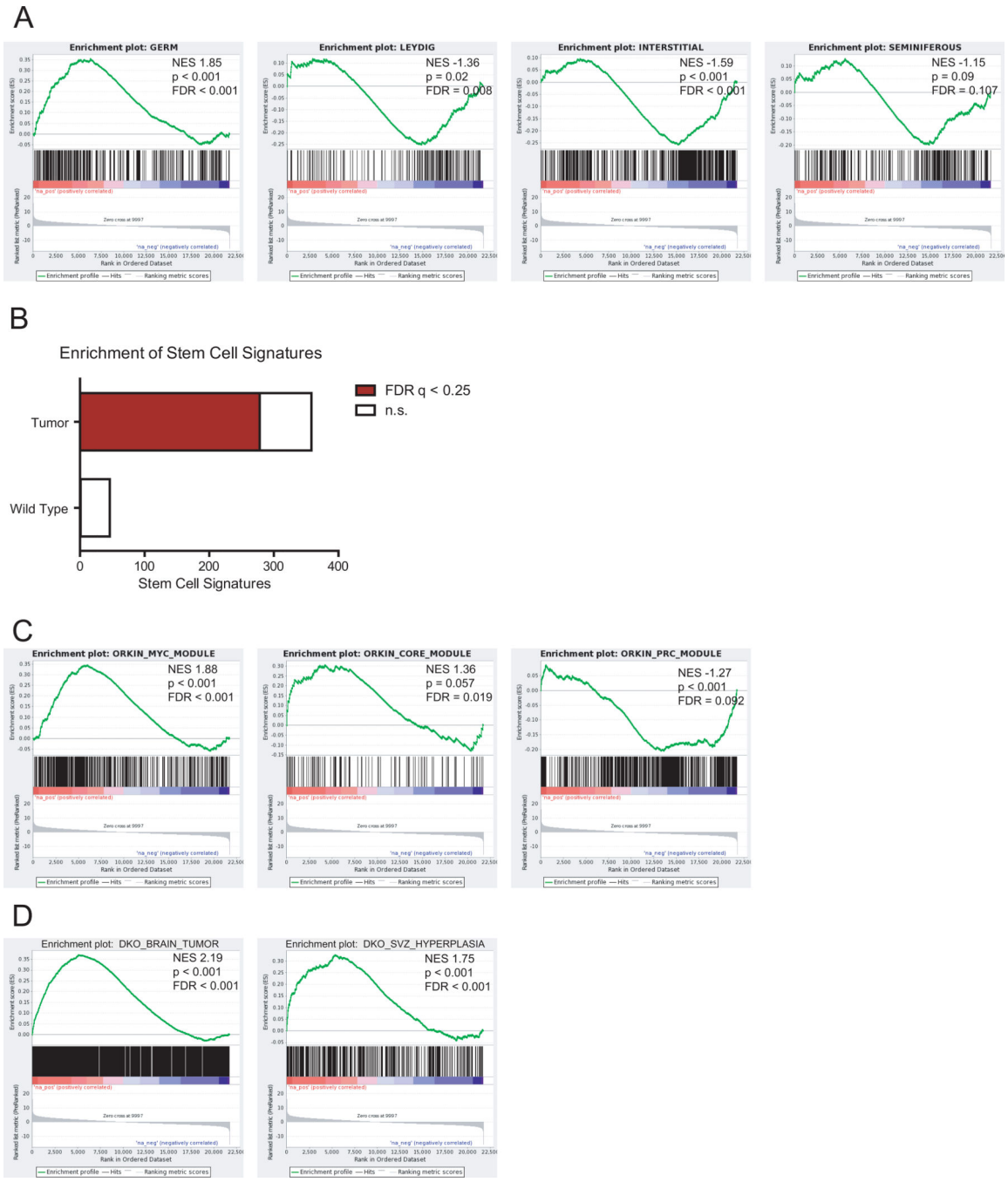

Figure 5.

Gene expression analysis of *Nestin*^{Cre}*Bax*$^{fl/fl}$*Bak*$^{-/-}$ tumors. (A) Gene expression profiling was performed on wild-type (n=2) and tumor-bearing *Nestin*^{Cre}*Bax*$^{fl/fl}$*Bak*$^{-/-}$ (n=4) testes. The testes tumors of *Nestin*^{Cre}*Bax*$^{fl/fl}$*Bak*$^{-/-}$ mice manifested a germ cell signature rather than a Leydig, interstitial, or seminiferous expression profile, as assessed by Gene Set Enrichment Analysis (GSEA). (B) Fraction of total and significant (FDR q <0.25) stem cell signatures enriched in either the wild-type or tumor-bearing *Nestin*^{Cre}*Bax*$^{fl/fl}$*Bak*$^{-/-}$ testes. (C) GSEA of wild-type vs. tumor-bearing *Nestin*^{Cre}*Bax*$^{fl/fl}$*Bak*$^{-/-}$ testes for the Myc, Core

and PrC signatures (26). (D) GSEA of wild-type vs. tumor-bearing *Nestin*^{Cre}*Bax*$^{fl/fl}$*Bak*$^{-/-}$ testes for the gene signatures derived from the *Nestin*^{Cre}*Bax*$^{fl/fl}$*Bak*$^{-/-}$ aggressive brain tumor or *Nestin*^{Cre}*Bax*$^{fl/fl}$*Bak*$^{-/-}$ brains bearing SVZ proliferations.